INTERLAMINAR STRESSES ANALYSIS OF THREE-DIMENSIONAL COMPOSITE LAMINATES BY THE BOUNDARY ELEMENT METHOD

Y. C. Shiah*

Department of Aeronautics and Astronautics
National Cheng Kung University
Tainan, Taiwan

M. R. Hematiyan

Department of Mechanical Engineering
Shiraz University
Shiraz, Iran

ABSTRACT

In engineering industries, composite laminates have been widely applied for various applications. This work presents an efficient analysis of the interlaminar stresses in three-dimensional thin layered anisotropic composites by the boundary element method (BEM). Due to the nearly singular integrals in the boundary integral equation, the conventional BEM approach cannot be applied to analyze the composite layers that are very thin. The present work employs the self-regularization scheme to analyze the interlaminar stresses in thin anisotropic composites. In the end, a few benchmark examples are presented to show the applicability of the present approach.

Keywords: Composite laminates, Interlaminar stresses, Boundary element method.

1. INTRODUCTION

Nowadays, a remarkable progress of industrial technologies has made extremely high demands of anisotropic composites to meet high-level requirements. For various purposes, composites are often constructed by combining two or more thin layers of anisotropic materials such that the combination of physically or chemically different phases may yield high performance to meet various requirements. However, one of the major concerns in the use of composites is the debonding of layers, to which a significant amount of researches have been devoted in the past. For examples, González-Cantero *et al*. [1] presented a new analytical model for evaluating interlaminar stresses in the unfolding failure of composite laminates. Using a three-dimensional multi-term extended Kantorovich method, Tahani and Andakhshideh [2] analyzed the bending of thick rectangular laminated plates with arbitrary laminations and boundary conditions. By this methodology, Tahani *et al*. [3] theoretically studied the interlaminar stresses in thick cylindrical shell with arbitrary laminations under transverse loads. The results obtained from this theory were compared with numerical or analytical results of the existing solutions in simplified cases. Also, Fu *et al*. [4] proposed an analytical solution to investigate interlaminar stresses for laminated shells with interfacial damage. Of course, there are too many other analytical works to mention here for a complete review. Despite the significant contributions of analytical works, analysis by numerical tools is generally necessary for engineering applications with complicated geometries and boundary conditions.

Among all numerical tools for engineering analysis, the finite element method (FEM) is perhaps the most commonly applied approach in engineering industries. In the FEM, shell elements can be applied to treat very thin structures only when shear stresses are negligibly small. For structures subjected to significant shears, three-dimensional solid elements are generally needed for the modeling. For analyzing the interlaminar stresses in multiply combined anisotropic composites, difficulties will arise for the FEM modeling when the thickness order of layers is extremely small as compared with the characteristic dimension of structures. Gener-

* Corresponding author (ycshiah@mail.ncku.edu.tw)

DOI : 10.1017/jmech.2018.8
Copyright © 2018 The Society of Theoretical and Applied Mechanics
https://doi.org/10.1017/jmech.2018.8 Published online by Cambridge University Press

ally speaking, the aspect ratio of 3D modeling elements needs to be confined no less than 1/20 to yield reliable results and thus, a relatively large amount of elements are required to model very thin layers when significant interlaminar shears are present. Another numerical tool- meshless method has also been widely applied to solve solid mechanics since its first study using the Smoothed Particle Hydrodynamics (SPH) by Libersky and Petschek [5]. Also, Barbieri has proposed Meshfree and Partition of Unity Methods to analyze composite materials [6]. As a powerful alternative, the boundary element method (BEM) has a very similar modeling difficulty but for another different reason. For treating thin layers, its use requires special attention because of the nearly singular characteristic of the kernels in the boundary integral equation (BIE). Nearly singular integration will occur whenever the source point on one surface approaches to the integration elements on the other side of the thin layer. Because of the rapid variations of the integrands under this condition, the conventional numerical integration scheme in BEM will generally fail to yield proper results unless a regularization scheme is adopted, without having to employ a very refined mesh.

Over the years, there are several regularization schemes proposed to treat the problem of nearly singular integrations (see e.g. [7-10]). Even though these approaches are very effective for treating either 2D or 3D problems modeled with plane elements, they are either analytically complex and/or relatively difficult to implement for general 3D problems. It is worth noting too that the above-mentioned works deal only with isotropic analyses; to treat 3D generally anisotropic problems in elastostatics, these regularization schemes of the boundary integrals will be even more challenging due to the additional mathematical complexity of the anisotropic Green's function. For dealing with thin bodies in particular, the methods hitherto reported in the BEM literature are mostly to regularize the kernels analytically (see e.g. [11-15]). Indeed, these schemes are mathematically involved and thus far from simple to implement for treating 3D generally anisotropic thin bodies. Another general scheme, often referred to as "self-regularization", has also been proposed by several authors (see e.g. [16-19]). Since this self-regularization scheme does not require the $C^{1,\alpha}$ Holder continuity of the boundary element being used, it is relatively simple to implement. For that, He and Tan [20] have implemented this scheme to the 3D isotropic elastostatic analysis. Following the work, Shiah *et al*. [21] further applied this scheme to treat 3D thin-walled anisotropic structures. Also, Shiah [22] has applied this technique to the analysis of near-boundary solution of 3D anisotropic elasticity. This article aims to apply this self-regularization approach to analyze the interlaminar stresses in composites made of thin anisotropic layers. Using this scheme, the analyses are carried out for a few benchmark examples to investigate their interlaminar stresses. Also, comparisons are made for the situation when thin epoxy layers are considered or not.

2. BEM TREATMENT OF COMPOSITE LAYERS

The present work targets the study of interlaminar stresses in thin layered composites by applying the BEM. For modeling layered structures, the conventional sub-region technique in the BEM is applied, where an assemblage of collocation equations for each layer is formulated into a matrix form using the well established BIE as follows:

$$C_{ij}(P)u_j(P)+\int_S u_j(Q)T_{ij}^*(P,Q)\,dS=\int_S t_j(Q)U_{ij}^*(P,Q)\,dS \qquad (i,j=1,2,3) \tag{1}$$

In Eq. (1), C_{ij} is the free term at the source point P; u_j and t_j are displacements and tractions at the field point Q on the surface S. All integrals in Eq. (1) are numerically computed, in which $U_{ij}^* \equiv \mathbf{U}^*$ and $T_{ij}^* \equiv \mathbf{T}^*$ represent the fundamental solutions of displacements and tractions, respectively, in the x_i-direction at the field point Q due to a unit load applied in the x_j-direction at P in a homogeneous infinite elastic body. For providing a clear picture about how we treat 3D anisotropic materials, the fundamental solutions are briefly outlined in what follows.

Being the first work of deriving the Green's function for 3D anisotropic medium, Lifschitz and Rosenzweig [23] presented $\mathbf{U}^*$ as a line integral around a unit circle about the source point on an oblique plane, with the integrand containing the Christoffel matrix defined in terms of elastic constants. Due to the costly computation efforts for evaluating the integral, numerous efforts have been devoted to reformulating it into simpler or more explicit analytical forms. Recently, Shiah *et al*. [24] and Tan *et al*. [25] found that the fully explicit expression for $\mathbf{U}^*$ derived by Ting and Lee [26] is very well suited indeed for implementation in the BEM. As derived by Ting and Lee [26], $\mathbf{U}^*$ can be computed in the spherical coordinate system (r, θ, ϕ) by

$$\mathbf{U}^*(\mathbf{x})=\frac{1}{4\pi r}\frac{1}{|\boldsymbol{\kappa}|}\sum_{\mathbf{n}=0}^{4}q_n\hat{\boldsymbol{\Gamma}}^{(\mathbf{n})} \tag{2}$$

where

$$q_n=\begin{cases}\dfrac{-1}{2\beta_1\beta_2\beta_3}\left[\mathrm{Re}\left\{\displaystyle\sum_{t=1}^{3}\frac{p_t^n}{(p_t-\overline{p}_{t+1})(p_t-\overline{p}_{t+2})}\right\}-\delta_{n2}\right] & \text{for } n=0,1,2,\\ \dfrac{1}{2\beta_1\beta_2\beta_3}\mathrm{Re}\left\{\displaystyle\sum_{t=1}^{3}\frac{p_t^{n-2}\overline{p}_{t+1}\overline{p}_{t+2}}{(p_t-\overline{p}_{t+1})(p_t-\overline{p}_{t+2})}\right\} & \text{for } n=3,4,\end{cases} \tag{3a}$$

$$\hat{\Gamma}_{ij}^{(n)}=\tilde{\Gamma}_{(i+1)(j+1)(i+2)(j+2)}^{(n)}-\tilde{\Gamma}_{(i+1)(j+2)(i+2)(j+1)}^{(n)} \tag{3b}$$

$$\kappa_{ik}=\tilde{C}_{ijks}m_j m_s,\quad \mathbf{m}=(-\sin\theta,\cos\theta,0) \tag{3c}$$

https://doi.org/10.1017/jmech.2018.8 Published online by Cambridge University Press

where $\tilde{C}_{ijks}$ is the stiffness matrix; pi are the Stroh eigenvalues, determined by solving the sextic equation $|\mathbf{\kappa}| = 0$ for the roots that appear as three pairs of complex conjugates, $p_v = \alpha_v + \mathbf{i}\beta_v$, where $\beta_v > 0$ and $i = \sqrt{(-1)}$. Further details of the algebraic expressions for $\tilde{\Gamma}^{(n)}_{pqrs}$ can be referred to Shiah *et al*. [24]. Despite the conciseness of Eq. (2), its derivatives in analytical forms are very complicated and thus pretty involved for their numerical evaluations. For simplifying the expressions of the derivatives, Tan *et al*. [27] proposed to represent U^* by a double Fourier series form as follows:

$$U^*_{uv}(r,\theta,\phi) = \frac{1}{4\pi r}\sum_{m=-\alpha}^{\alpha}\sum_{n=-\alpha}^{\alpha}\lambda^{(m,n)}_{uv}e^{\mathbf{i}(m\theta+n\phi)} \tag{4}$$

where the coefficients $\lambda^{(m,n)}_{uv}$ are evaluated by

$$\lambda^{(m,n)}_{uv} = \frac{1}{4\pi^2}\int_{-\pi}^{\pi}\int_{-\pi}^{\pi}\frac{1}{|\mathbf{\kappa}|}\sum_{n=0}^{4}q_n\hat{\mathbf{\Gamma}}^{(n)}e^{-\mathbf{i}(m\theta+n\phi)}d\theta d\phi. \tag{5}$$

To expedite the computational efficiency, Shiah *et al*. [28] separates $\lambda^{(m,n)}_{uv}$ into its real part $R^{(m,n)}_{uv}$ and imaginary part $I^{(m,n)}_{uv}$. By using the feature that $\lambda^{(m,n)}_{uv}$ and $\lambda^{(-m,-n)}_{uv}$ are complex conjugates, Eq. (4) can be rewritten as [28]

$$\begin{aligned}U^*_{uv} = \frac{1}{2\pi r}\Bigg\{&\sum_{m=1}^{\alpha}\sum_{n=1}^{\alpha}\Big[\big(\tilde{R}^{(m,n)}_{uv}\cos m\theta - \tilde{I}^{(m,n)}_{uv}\sin m\theta\big)\cos n\phi - \big(\tilde{R}^{(m,n)}_{uv}\sin m\theta + \tilde{I}^{(m,n)}_{uv}\cos m\theta\big)\sin n\phi\Big]\\ &+\sum_{m=1}^{\alpha}\big(R^{(0,m)}_{uv}\cos m\phi - I^{(0,m)}_{uv}\sin m\phi + R^{(m,0)}_{uv}\cos m\theta - I^{(m,0)}_{uv}\sin m\theta\big) + \frac{R^{(0,0)}_{uv}}{2}\Bigg\},\end{aligned} \tag{6}$$

where

$$\tilde{R}^{(m,n)}_{uv} = R^{(m,n)}_{uv} + R^{(m,-n)}_{uv},\quad \hat{R}^{(m,n)}_{uv} = R^{(m,n)}_{uv} - R^{(m,-n)}_{uv},\quad \tilde{I}^{(m,n)}_{uv} = I^{(m,n)}_{uv} + I^{(m,-n)}_{uv},\quad \hat{I}^{(m,n)}_{uv} = I^{(m,n)}_{uv} - I^{(m,-n)}_{uv}. \tag{7}$$

Using the chain rule to take the spatial derivatives of Eq. (6), the 1st-order derivatives of the Green's function are given by [28]

$$U^*_{uv,l} = \frac{1}{2\pi r^2}\begin{Bmatrix}-\omega_l(\theta,\phi)\Big[\sum_{m=1}^{\alpha}\sum_{n=1}^{\alpha}\big(\tilde{\Gamma}^{(m,n)}_{uv}(\theta)\cos n\phi - \breve{\Gamma}^{(m,n)}_{uv}(\theta)\sin n\phi\big) + \sum_{m=1}^{\alpha}\big(\tilde{\gamma}^{m}_{uv}(\theta) + \breve{\gamma}^{m}_{uv}(\phi)\big) + \frac{R^{(0,0)}_{uv}}{2}\Big]\\ -\omega'_l(\theta,\phi)\Big[\sum_{m=1}^{\alpha}\sum_{n=1}^{\alpha}m\big(\tilde{\Gamma}^{(m,n)}_{uv}(\theta)\cos n\phi + \hat{\Gamma}^{(m,n)}_{uv}(\theta)\sin n\phi\big) + \sum_{m=1}^{\alpha}m\cdot\tilde{\gamma}^{m}_{uv}(\theta)\Big]\\ -\omega''_l(\theta,\phi)\Big[\sum_{m=1}^{\alpha}\sum_{n=1}^{\alpha}n\big(\hat{\Gamma}^{(m,n)}_{uv}(\theta)\sin n\phi + \breve{\Gamma}^{(m,n)}_{uv}(\theta)\cos n\phi\big) + \sum_{m=1}^{\alpha}m\cdot\hat{\gamma}^{m}_{uv}(\phi)\Big]\end{Bmatrix}, \tag{8}$$

where

$$\omega_l(\theta,\phi) = r\frac{\partial r}{\partial x_l} = \begin{cases}\sin\phi\cos\theta, & (\text{for } l=1)\\ \sin\phi\sin\theta, & (\text{for } l=2)\\ \cos\phi, & (\text{for } l=3)\end{cases}, \tag{9a}$$

$$\omega'_l(\theta,\phi) = r\frac{\partial \theta}{\partial x_l} = \begin{cases}-\sin\theta/\sin\phi, & (\text{for } l=1)\\ \cos\theta/\sin\phi, & (\text{for } l=2)\\ 0, & (\text{for } l=3)\end{cases}, \tag{9b}$$

https://doi.org/10.1017/jmech.2018.8 Published online by Cambridge University Press

$$\omega_l''(\theta,\phi)=r\frac{\partial\phi}{\partial x_l}=\begin{cases}\cos\phi\cos\theta, & (\text{for } l=1)\\ \cos\phi\sin\theta, & (\text{for } l=2)\\ -\sin\phi, & (\text{for } l=3)\end{cases}, \tag{9c}$$

$$\breve{\Gamma}_{uv}^{(m,n)}(\theta)=\tilde{R}_{uv}^{(m,n)}\cos m\theta-\tilde{I}_{uv}^{(m,n)}\sin m\theta,\quad \breve{\Gamma}_{uv}^{(m,n)}(\theta)=\hat{R}_{uv}^{(m,n)}\sin m\theta+\hat{I}_{uv}^{(m,n)}\cos m\theta,$$

$$\tilde{\Gamma}_{uv}^{(m,n)}(\theta)=\tilde{R}_{uv}^{(m,n)}\sin m\theta+\tilde{I}_{uv}^{(m,n)}\cos m\theta,\quad \hat{\Gamma}_{uv}^{(m,n)}(\theta)=\hat{R}_{uv}^{(m,n)}\cos m\theta-\hat{I}_{uv}^{(m,n)}\sin m\theta,$$

$$\breve{\gamma}_{uv}^{m}(\theta)=R_{uv}^{(m,0)}\cos m\theta-I_{uv}^{(m,0)}\sin m\theta,\quad \breve{\gamma}_{uv}^{m}(\phi)=R_{uv}^{(0,m)}\cos m\phi-I_{uv}^{(0,m)}\sin m\phi,$$

$$\tilde{\gamma}_{uv}^{m}(\theta)=R_{uv}^{(m,0)}\sin m\theta-I_{uv}^{(m,0)}\cos m\theta,\quad \hat{\gamma}_{uv}^{m}(\phi)=R_{uv}^{(0,m)}\sin m\phi+I_{uv}^{(0,m)}\cos m\phi. \tag{9d}$$

From the formulations provided above, it is clear that computations of the 1st order derivatives are computation-wise very efficient indeed. Having obtained the values of the derivatives, one may then directly calculate $\mathbf{T}^*$ by

$$T_{ij}^*=\tilde{C}_{ikmn}\left(U_{mj,n}^*+U_{nj,m}^*\right)\bar{n}_k/2. \tag{10}$$

From the fundamental solutions of $\mathbf{U}^*$ and $\mathbf{T}^*$ (for either isotropic or anisotropic medium), it is apparent to see their singular nature when r approaches zero. As a consequence, any conventional scheme to numerically compute the integrals with these solutions in the integrands will certainly result in incorrect values. Due to this, evaluations of the boundary integrals need to be specially treated when the analyzed structures are very thin as compared with their characteristic dimension. Typically, this happens to the present case under study, that is, thin layered composites. For this case, self-regularization of the displacement BIE to yield proper values will be reviewed next.

3. SELF-REGULARIZED BIE

As can be clearly identified, the fundamental solutions of $\mathbf{U}^*$ and $\mathbf{T}^*$ appear to singularities of the orders r^{-1} and r^{-2}, respectively. As aforementioned, this leads to difficulties in proper numerical evaluations of the boundary integrals for treating a thin body. As presented by He and Tan [20], for a reference point $\hat{P}$ on the surface, the self-regularized BIE is expressed as

$$C_{ij}(P)\left[u_j(P)-u_j^L(\hat{P},P)\right]+\int_S T_{ij}^*(P,Q)\left[u_j(Q)-u_j^L(\hat{P},Q)\right]dS=\int_S U_{ij}^*(P,Q)\left[t_j(Q)-t_j^L(\hat{P},Q)\right]dS, \tag{11}$$

where $u_i^L(\hat{P},Q)$ and $t_i^L(\hat{P},Q)$ represent the local displacements and tractions at Q under the constant-stress state at $\hat{P}$, respectively. In Eq. (11), $u_i^L(\hat{P},P\setminus Q)$ and $t_i^L(\hat{P},Q)$ under the constant stress state are given by

$$u_j^L(\hat{P},P\setminus Q)=u_j(\hat{P})+u_{j,m}(\hat{P})\left[x_m(P\setminus Q)-x_m(\hat{P})\right], \tag{12a}$$

$$t_j^L(\hat{P},Q)=\frac{\tilde{C}_{jmst}}{2}\left[u_{s,t}(\hat{P})+u_{t,s}(\hat{P})\right]\bar{n}_m(Q). \tag{12b}$$

Under the constant-stress state, the displacement gradients at $\hat{P}$ in Eq. (12a) are constants that can be determined by solving the following equation:

$$\left[t_1\ t_2\ t_3\ \underline{u}_{1,1}\ \underline{u}_{1,2}\ \underline{u}_{2,1}\ \underline{u}_{2,2}\ \underline{u}_{3,1}\ \underline{u}_{3,2}\right]^T=\left[A_{mn}\right]\left[u_{1,1}\ u_{1,2}\ u_{1,3}\ u_{2,1}\ u_{2,2}\ u_{2,3}\ u_{3,1}\ u_{3,2}\ u_{3,3}\right]^T, \tag{13}$$

where the underline for the displacement gradients is used to denote the local coordinate system (ξ_1,ξ_2); the non-zero elements of A_{mn} for an anisotropic body are given by [21]

https://doi.org/10.1017/jmech.2018.8 Published online by Cambridge University Press

$$A_{11}=C_{11}\overline{n}_1+C_{61}\overline{n}_2+C_{51}\overline{n}_3,\quad A_{12}=C_{16}\overline{n}_1+C_{66}\overline{n}_2+C_{56}\overline{n}_3,\quad A_{13}=C_{15}\overline{n}_1+C_{65}\overline{n}_2+C_{55}\overline{n}_3,$$

$$A_{14}=C_{16}\overline{n}_1+C_{66}\overline{n}_2+C_{56}\overline{n}_3,\quad A_{15}=C_{12}\overline{n}_1+C_{62}\overline{n}_2+C_{52}\overline{n}_3,\quad A_{16}=C_{14}\overline{n}_1+C_{64}\overline{n}_2+C_{54}\overline{n}_3,$$

$$A_{17}=C_{15}\overline{n}_1+C_{65}\overline{n}_2+C_{55}\overline{n}_3,\quad A_{18}=C_{14}\overline{n}_1+C_{64}\overline{n}_2+C_{54}\overline{n}_3,\quad A_{19}=C_{13}\overline{n}_1+C_{63}\overline{n}_2+C_{53}\overline{n}_3,$$

$$A_{21}=C_{61}\overline{n}_1+C_{21}\overline{n}_2+C_{41}\overline{n}_3,\quad A_{22}=C_{66}\overline{n}_1+C_{26}\overline{n}_2+C_{46}\overline{n}_3,\quad A_{23}=C_{65}\overline{n}_1+C_{25}\overline{n}_2+C_{45}\overline{n}_3,$$

$$A_{24}=C_{66}\overline{n}_1+C_{26}\overline{n}_2+C_{46}\overline{n}_3,\quad A_{25}=C_{62}\overline{n}_1+C_{22}\overline{n}_2+C_{42}\overline{n}_3,\quad A_{26}=C_{64}\overline{n}_1+C_{24}\overline{n}_2+C_{44}\overline{n}_3,$$

$$A_{27}=C_{65}\overline{n}_1+C_{25}\overline{n}_2+C_{45}\overline{n}_3,\quad A_{28}=C_{64}\overline{n}_1+C_{24}\overline{n}_2+C_{44}\overline{n}_3,\quad A_{29}=C_{63}\overline{n}_1+C_{23}\overline{n}_2+C_{43}\overline{n}_3,$$

$$A_{31}=C_{51}\overline{n}_1+C_{41}\overline{n}_2+C_{31}\overline{n}_3,\quad A_{32}=C_{56}\overline{n}_1+C_{46}\overline{n}_2+C_{36}\overline{n}_3,\quad A_{33}=C_{55}\overline{n}_1+C_{45}\overline{n}_2+C_{35}\overline{n}_3,$$

$$A_{34}=C_{56}\overline{n}_1+C_{46}\overline{n}_2+C_{36}\overline{n}_3,\quad A_{35}=C_{52}\overline{n}_1+C_{42}\overline{n}_2+C_{32}\overline{n}_3,\quad A_{36}=C_{54}\overline{n}_1+C_{44}\overline{n}_2+C_{34}\overline{n}_3,$$

$$A_{37}=C_{55}\overline{n}_1+C_{45}\overline{n}_2+C_{35}\overline{n}_3,\quad A_{38}=C_{54}\overline{n}_1+C_{44}\overline{n}_2+C_{34}\overline{n}_3,\quad A_{39}=C_{53}\overline{n}_1+C_{43}\overline{n}_2+C_{33}\overline{n}_3,$$

$$A_{41}=x_{\underline{1,1}},\quad A_{42}=x_{\underline{2,1}},\quad A_{43}=x_{\underline{3,1}},\quad A_{54}=x_{\underline{1,1}},\quad A_{55}=x_{\underline{2,1}},\quad A_{56}=x_{\underline{3,1}},$$

$$A_{67}=x_{\underline{1,1}},\quad A_{68}=x_{\underline{2,1}},\quad A_{69}=x_{\underline{3,1}},\quad A_{71}=x_{\underline{1,2}},\quad A_{73}=x_{\underline{3,2}},\quad A_{74}=x_{\underline{2,2}},$$

$$A_{84}=x_{\underline{1,2}},\quad A_{85}=x_{\underline{2,2}},\quad A_{86}=x_{\underline{3,2}},\quad A_{97}=x_{\underline{1,2}},\quad A_{98}=x_{\underline{2,2}},\quad A_{99}=x_{\underline{3,2}}. \tag{14}$$

In Eq. (14), C_{ij} is the contracted notation of $\tilde{C}_{mnst}$. The $x_{\underline{i,j}}$ in Eq. (14) represents $\partial x_i/\partial\xi_j$, given by

$$\frac{\partial x_i}{\partial \xi_j}=\sum_{c=1}^{8\text{ or }6}\frac{\partial N^{(c)}(\xi_1^{\hat{P}},\xi_2^{\hat{P}})}{\partial \xi_j}x_i^{(c)}, \tag{15}$$

where $x_i^{(c)}$ are the coordinates of the c–th node of the element where $\hat{P}$ is located and $(\xi_1^{\hat{P}},\xi_2^{\hat{P}})$ are the local coordinates of $\hat{P}$; c has a range of 1–8 for a quadrilateral element and 1–6 for a triangular element. With matrix inversion of Eq. (14), the displacement gradients at $\hat{P}$ are now given by

$$u_{i,j}(\hat{P})=A^{-1}_{3i+j-3,s}t_s(\hat{P})+A^{-1}_{3i+j-3,t+2k+1}u_{\underline{k,t}}(\hat{P}),\quad (s,k=1,2,3;\ t=1,2) \tag{16}$$

where $A^{-1}_{m,n}$ are the elements of $\mathbf{A}^{-1}$. In Eq. (16), the local tractions and displacement gradients at $\hat{P}$ are determined by interpolation of nodal tractions and nodal displacements using the shape functions $N^{(c)}$, i.e.

$$t_s(\hat{P})=\sum_{c=1}^{8\text{ or }6}N^{(c)}(\xi_1^{\hat{P}},\xi_2^{\hat{P}})t_s^{(c)},\quad u_{\underline{i,s}}(\hat{P})=\sum_{c=1}^{8\text{ or }6}\frac{\partial N^{(c)}(\xi_1^{\hat{P}},\xi_2^{\hat{P}})}{\partial \xi_s}u_i^{(c)}, \tag{17}$$

As a result of substituting Eqs. (16) and (17) into Eqs. (12a) and (12b), one obtains

$$u_i^L(\hat{P},P\backslash Q)=\sum_{c=1}^{8\text{ or }6}N^{(c)}(\xi_1^{\hat{P}},\xi_2^{\hat{P}})u_i^{(c)}+\begin{pmatrix}A^{-1}_{3i+m-3,s}\sum_{c=1}^{8\text{ or }6}N^{(c)}(\xi_1^{\hat{P}},\xi_2^{\hat{P}})t_s^{(c)}\\ +A^{-1}_{3i+m-3,s+3}\sum_{c=1}^{8\text{ or }6}N_s'^{(c)}(\xi_1^{\hat{P}},\xi_2^{\hat{P}})u_1^{(c)}\\ +A^{-1}_{3i+m-3,s+6}\sum_{c=1}^{8\text{ or }6}N_s'^{(c)}(\xi_1^{\hat{P}},\xi_2^{\hat{P}})u_2^{(c)}\end{pmatrix}\left[x_m(P\backslash Q)-\sum_{c=1}^{8\text{ or }6}N^{(c)}(\xi_1^{\hat{P}},\xi_2^{\hat{P}})x_m^{(c)}\right], \tag{18a}$$

$$t_i^L(\hat{P},Q)=\frac{\tilde{C}_{imst}}{2}\begin{bmatrix}\left(A^{-1}_{3s+t-3,k}+A^{-1}_{3t+s-3,k}\right)\sum_{c=1}^{8\text{ or }6}N^{(c)}(\xi_1^{\hat{P}},\xi_2^{\hat{P}})t_k^{(c)}\\ +\left(A^{-1}_{3s+t-3,k+3}+A^{-1}_{3t+s-3,k+3}\right)\sum_{c=1}^{8\text{ or }6}N_k'^{(c)}(\xi_1^{\hat{P}},\xi_2^{\hat{P}})u_1^{(c)}\\ +\left(A^{-1}_{3s+t-3,k+6}+A^{-1}_{3t+s-3,k+6}\right)\sum_{c=1}^{8\text{ or }6}N_k'^{(c)}(\xi_1^{\hat{P}},\xi_2^{\hat{P}})u_2^{(c)}\end{bmatrix}\overline{n}_m(Q), \tag{18b}$$

https://doi.org/10.1017/jmech.2018.8 Published online by Cambridge University Press

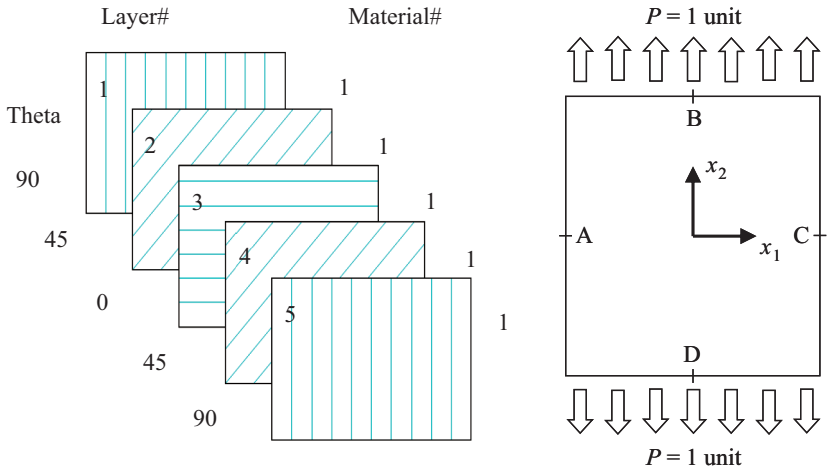


Fig. 1 A symmetrically laminated composite subjected to uniaxial tension.

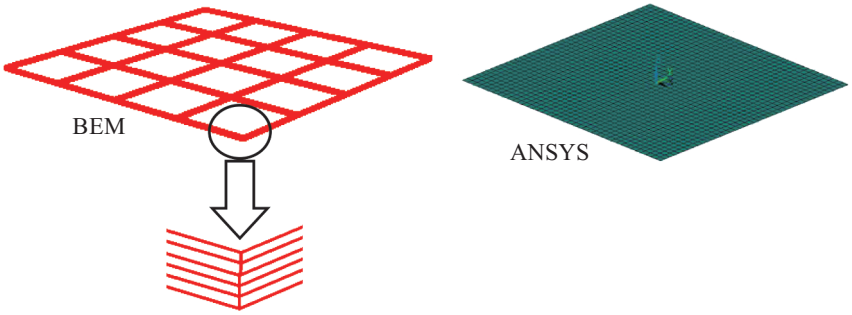


Fig. 2 Modeling of the symmetrically laminated composite subjected to uniaxial tension.

where $N_k^{\prime(c)}$ denotes the 1st-order derivative of $N^{(c)}$ with respect to ξ_k. The local coordinates of $\hat{P}$, i.e. $(\xi_1^{\hat{P}}, \xi_2^{\hat{P}})$, can be easily determined from the geometrical relation that the vector $\overline{P\hat{P}}$ is always perpendicular to the tangent plane at the regularization point with local coordinates $(\xi_1^{\hat{P}}, \xi_2^{\hat{P}})$.

Using Eqs. (18a)-(18b) substituted into Eq. (11), one may directly integrate the boundary integrals in the self-regularized BIE by any conventional scheme, e.g. the Gauss quadrature rule, to formulate a system of simultaneous equations for each layer of the composite. By the conventional sub-region technique in the BEM, one may then solve the boundary integral equation for unknown boundary values.

4. NUMERICAL EXAMPLES

By the sub-region technique of the BEM treatment, all interlaminar stresses can thus be determined. In this work, this technique is implemented in an existing BEM code, based on quadratic isoparametric elements, to study the interlaminar stresses of thin layered anisotropic composites. To show the validity of our BEM analysis, the first case treats an example that has analytical solution, i.e. a symmetrically laminated 4 (unit) × 4 (unit) composite with cross-ply angles $[90^0/45^0/0^0/45^0/90^0]$ subjected to uniaxial unit tension (P = 1 unit) as shown in Fig. 1. The material is Glass/Epoxy with each layer thickness equal to 0.01 (unit).

As shown in Fig. 1, points A, C are constrained in the x_2 and x_3-direction, and point B constrained in the x_1 and x_3-direction. The material properties of Glass/Epoxy used for the analysis are

$$E_1 = 34.5(GPa), \quad E_2 = 51.6(GPa), \quad E_3 = 25(GPa),$$
$$\nu_{12} = 0.28, \quad \nu_{23} = 0.28, \quad \nu_{13} = 0.3,$$
$$G_{12} = 3.7(GPa), \quad G_{23} = 62(GPa), \quad G_{31} = 6.3(GPa). \quad (20)$$

Despite the symmetrical conditions, the BEM analysis still employs full modeling since the same model will be used for the later analysis of asymmetrically laminated composite. Also, the problem was analyzed using the FEM-based software ANSYS that will be used for the later analysis of more numerical examples. Figure 2 shows the modeling of the both approaches by BEM (240 quadratic elements with 730 nodes) and ANSYS (1600 SHELL281 elements with 4961 nodes). Analytical solution to this example can be referred to [29].

The calculated displacements along the mid-plane BD

https://doi.org/10.1017/jmech.2018.8 Published online by Cambridge University Press

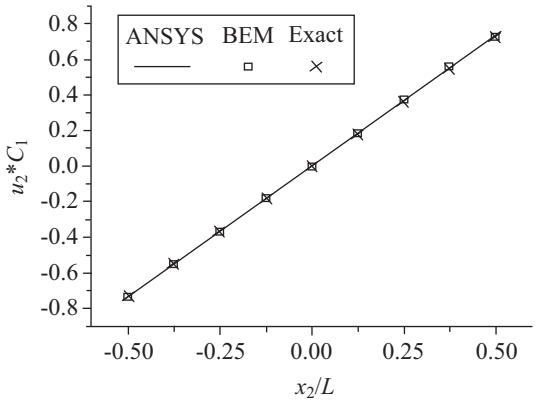


Fig. 3 Displacements along BD for the symmetrically laminated composite.

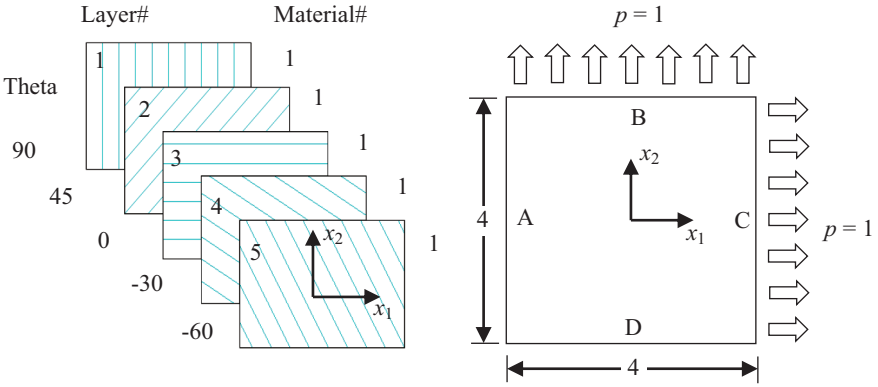


Fig. 4 Asymmetrical laminated composite subjected to bi-tension.

are plotted in Fig. 3. As can be seen from the plot, all solutions agree with one another pretty well.

To further show the applicability of the implemented code for treating general cross-ply laminates, the second example deals with the previous square plate but laminated asymmetrically with cross-ply angles $[90^0/45^0/0^0/-30^0/-60^0]$ (Fig. 4). Suppose the asymmetrically laminated composite is subjected to unit tension ($P = 1$ unit) on sides B and C; sides A, D, and the bottom surface on layer#1 are constrained from motion in their normal directions as indicated in Fig. 4. Since no analytical solution exists for this problem, the FEM analysis by ANSYS was also performed for validating our BEM results. The same modeling meshes were used for both BEM and ANSYS analysis as in the previous analysis (Fig. 2). The calculated total displacements ($u_0 = \sqrt{u_1^2 + u_2^2 + u_3^2}$) on the mid-plane along $x_2 = 0$ were plotted in Fig. 5 for their normalized values. Once again, pretty consistent results are obtained. Also, the normalized equivalent stresses (σ_0/P) on this plane were calculated and listed in Table 1. It can be seen that the BEM results are indeed in good agreement with the analysis by ANSYS with only minor discrepancy due to modeling.

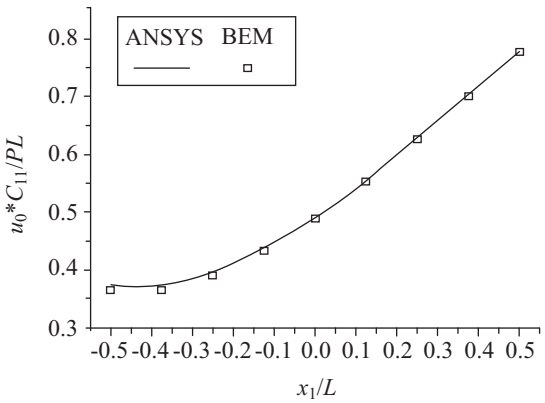


Fig. 5 Displacements on the mid-plane $x_2 = 0$ for the asymmetrically laminated composite.

5. CONCLUSIONS

One of the major concerns in the use of multi-layered composites is the potential debonding of layers. This paper presents an efficient technique for modeling of thin multi-layered composites by the BEM, where only very

https://doi.org/10.1017/jmech.2018.8 Published online by Cambridge University Press

Table 1 Equivalent stresses in each layer of the asymmetrically laminated composite.

	Layer#1		Layer#2		Layer#3		Layer#4		Layer#5	
x_1/L	ANSYS	BEM	ANSYS	BEM	ANSYS	BEM	ANSYS	BEM	ANSYS	BEM
-0.500	1.03E+00	9.89E-01 (3.84%)	1.07E+00	9.89E-01 (3.39%)	1.05E+00	1.08E+00 (2.47%)	1.02E+00	1.02E+00 (0.65%)	1.01E+00	1.01E+00 (0.15%)
-0.375	1.03E+00	1.03E+00 (0.07%)	1.06E+00	1.03E+00 (0.27%)	1.05E+00	1.05E+00 (0.12%)	1.03E+00	1.03E+00 (0.02%)	1.02E+00	1.02E+00 (0.00%)
-0.250	1.03E+00	1.02E+00 (0.67%)	1.05E+00	1.02E+00 (1.15%)	1.04E+00	1.03E+00 (0.84%)	1.03E+00	1.02E+00 (0.43%)	1.02E+00	1.02E+00 (0.35%)
-0.125	1.03E+00	1.03E+00 (0.40%)	1.05E+00	1.03E+00 (0.53%)	1.04E+00	1.03E+00 (0.54%)	1.03E+00	1.02E+00 (0.44%)	1.02E+00	1.02E+00 (0.36%)
0.000	1.03E+00	1.03E+00 (0.33%)	1.04E+00	1.03E+00 (0.33%)	1.03E+00	1.03E+00 (0.45%)	1.02E+00	1.02E+00 (0.45%)	1.02E+00	1.02E+00 (0.39%)
0.125	1.03E+00	1.03E+00 (0.36%)	1.04E+00	1.03E+00 (0.32%)	1.03E+00	1.02E+00 (0.39%)	1.02E+00	1.02E+00 (0.40%)	1.02E+00	1.02E+00 (0.37%)
0.250	1.03E+00	1.03E+00 (0.47%)	1.05E+00	1.03E+00 (0.69%)	1.02E+00	1.02E+00 (0.66%)	1.01E+00	1.01E+00 (0.51%)	1.02E+00	1.01E+00 (0.47%)
0.375	1.03E+00	1.03E+00 (0.47%)	1.05E+00	1.03E+00 (0.65%)	1.02E+00	1.02E+00 (0.37%)	1.01E+00	1.01E+00 (0.20%)	1.02E+00	1.01E+00 (0.15%)
0.500	9.91E-01	9.90E-01 (0.06%)	9.90E-01	9.90E-01 (4.49%)	1.02E+00	1.06E+00 (2.98%)	1.02E+00	9.95E-01 (2.28%)	1.03E+00	1.03E+00 (0.18%)

coarse meshes are required. Like domain solution techniques, the conventional BEM needs to employ very refined meshes to model thin layers of structures. This work applies the technique of self-regularization to model thin multi-layered composites. The major merit of this technique is the less mathematical treatments required and easy implementation in program code. Using the modeling proposed in this article, potential fracture can be efficiently and accurately assessed without heavy modeling efforts involved; even the computational time is much less than that of conventional techniques. Also, this technique can be further applied to the analysis of structures with thin coatings such that possible debonding of coatings can be efficiently assessed and prevented. Indeed, the proposed modeling technique is ideal to be applied to analyze interlaminar stresses in thin multi-layered composites.

ACKNOWLEDGEMENTS

The authors gratefully acknowledge the financial support from the Ministry of Science and Technology, R.O.C. (No. 106-2221-E-006-129).

REFERENCES

1. González-Cantero, J. M., Graciani, E., Blázquez, A. and París, F., "A New Analytical Model for Evaluating Interlaminar Stresses in the Unfolding Failure of Composite Laminates," *Composite Structures*, **147**, pp. 260-273 (2016).
2. Tahani, M. and Andakhshideh, A., "Interlaminar Stresses in Thick Rectangular Laminated Plates with Arbitrary Laminations and Boundary Conditions under Transverse Loads," *Composite Structures*, **94**, pp. 1793-1804 (2012).
3. Tahani, M., Andakhshideh, A. and Maleki, S., "Interlaminar Stresses in Thick Cylindrical Shell with Arbitrary Laminations and Boundary Conditions under Transverse Loads," *Composites Part B-Engineering*, **98**, pp. 151-165 (2016).
4. Fi, Y., Li, S. and Mao, Y., "The Analysis of Interlaminar Stresses for Composite Laminated Shallow Shells with Interfacial Damage," *Acta Mechanica Solida Sinica*, **24**, pp. 539-555 (2011).
5. Libersky, L. and Petschek, A., "Smooth Particle Hydrodynamics with Strength of Materials," *Proceedings of the Next Free-Lagrange Conference*, Jackson Lake Lodge, Moran, Wyoming (1990).
6. Barbieri, E. and Meo, M., "A Meshfree Penalty-Based Approach to Delamination in Composites," *Composites Science and Technology*, **69**, pp. 2169-2177 (2009).
7. Ma, H. and Kamiya, N., "A General Algorithm for Accurate Computation of Field Variables and Its Derivatives Near the Boundary in BEM," *Engineering Analysis with Boundary Element Method*, **25**, pp. 833-841 (2001).
8. Niu, Z., Wendland, W. L., Wang, X. and Zhou, H., "A Semi-Analytical Algorithm for the Evaluation of the Nearly Singular Integrals in Three-Dimensional Boundary Element Methods," *Computer Methods in Applied Mechanics and Engineering*, **194**, pp. 1057-1074 (2005).
9. Zhou, H. L., Niu, Z. R., Cheng, C. Z. and Guan, Z. W., "Analytical Integral Algorithm Applied to Boundary Layer Effect and Thin Body Effect in BEM for Anisotropic Potential Problems," *Compo-*

https://doi.org/10.1017/jmech.2018.8 Published online by Cambridge University Press

site Structures, **86**, pp. 1656-1671 (2008).

10. Shiah, Y. C., "3D Elastostatic Boundary Element Analysis of Thin Bodies by Integral Regularizations," *Journal of Mechanics*, **31**, pp. 533-543 (2014).
11. Ye, T. Q. and Liu, Y. J., "Finite Deflection Analysis of Elastic Plate by the Boundary Element Method," *Applied Mathematical Modelling*, **9**, pp. 183-188 (1985).
12. Liu, Y. J., "Elastic Stability Analysis of Thin Plate by the Boundary Element Method – A New Formulation," *Engineering Analysis with Boundary Element Method*, **4**, pp. 160-164 (1987).
13. Krishnasamy, G., Rizzo, F. J. and Li, Y. J., "Boundary Integral Equations for Thin Bodies," *International Journal for Numerical Methods in Engineering,* **37**, pp. 107-121 (1994).
14. Liu, Y. J., "Analysis of Shell-Like Structures by the Boundary Element Method Based on 3-D Elasticity: Formulation and Verification," *International Journal for Numerical Methods in Engineering,* **41**, pp. 541-558 (1998).
15. Cruse, T. A. and Aithal, R., "Non-Singular Boundary Integral Equation Implementation," *International Journal for Numerical Methods in Engineering*, **36**, pp. 237-254 (1993).
16. Rudolphi, T. J., "The Use of Simple Solutions in the Regularization of Hypersingular Boundary Integral Equations," *Mathematical and Computer Modeling*, **15**, pp. 269-278 (1991).
17. Sladek, V., Sladek, J. and Tanaka, M., "Regularization of Hypersingular and Nearly Singular Integrals in Potential Theory and Elasticity," *International Journal for Numerical Methods in Engineering,* **36**, pp. 1609-1628 (1993).
18. Matsumoto, T. and Tanaka, M., "Boundary Stress Calculation Using Regularized Boundary Integral Equation for Displacement Gradients," *International Journal for Numerical Methods in Engineering*, **36**, pp. 783-797 (1993).
19. Cruse, T. A. and Richardson, J. D., "Non-Singular Somigliana Stress Identities in Elasticity," *International Journal for Numerical Methods in Engineering*, **39**, pp. 3273-3304 (1996).
20. He, M. G. and Tan, C. L., "A Self-Regularization Technique in Boundary Element Method for 3-D Stress Analysis," *CMES-Computer Modeling in Engineering & Sciences*, **95**, pp. 317-349 (2013).
21. Shiah, Y. C., Tan, C. L. and Chan, L. D., "Boundary Element Analysis of Thin Anisotropic Structures by the Self-Regularization Scheme," *CMES-Computer Modeling In Engineering & Sciences*, **109**, pp. 15-33 (2015).
22. Shiah, Y. C. and Chang, L. D., "Boundary Element Calculation of Near-Boundary Solutions in 3D Generally Anisotropic Solids by the Self-Regularization Scheme," *Journal of Mechanics* DOI: 10.1017/jmech.2017.75 (2017).
23. Lifshitz, I. M. and Rozenzweig, L. N., "Construction of the Green Tensor for the Fundamental Equation of Elasticity Theory in the Case of Unbounded Elastically Anisotropic Medium," *Zhurnal Eksperimental noi I Teioretical Fiziki*, **17**, pp. 783-791 (1947).
24. Shiah, Y. C., Tan, C. L. and Lee, V. G., "Evaluation of Explicit-Form Fundamental Solutions for Displacements and Stresses in 3D Anisotropic Elastic Solids," *CMES-Computer Modeling in Engineering & Sciences*, **34**, pp. 205-226 (2008).
25. Tan, C. L., Shiah, Y. C. and Lin, C. W., "Stress Analysis of 3D Generally Anisotropic Solids Using the Boundary Element Method," *CMES-Computer Modeling in Engineering & Sciences*, **41**, pp. 195-214 (2009).
26. Ting, T. C. T. and Lee, V. G., "The Three-Dimensional Elastostatic Green's Function for General Anisotropic Linear Elastic Solid," *The Quarterly Journal of Mechanics and Applied Mathematics*, **50**, pp. 407-426 (1997).
27. Tan, C. L., Shiah, Y. C. and Wang, C. Y., "Boundary Element Elastic Stress Analysis of 3D Generally Anisotropic Solids Using Fundamental Solutions Based on Fourier Series," *International Journal of Solids And Structures*, **50**, pp. 2701-2711 (2013).
28. Shiah, Y. C., Tan, C. L. and Wang, C. Y., "An Improved Numerical Evaluation Scheme of the Fundamental Solution and Its Derivatives for 3D Anisotropic Elasticity Based on Fourier Series," *CMES-Computer Modeling in Engineering & Sciences*, **87**, pp. 1-22 (2012).
29. Hwu, C. B. and Chang, H. W., "Coupled Stretching–Bending Analysis of Laminated Plates with Corners via Boundary Elements," *Composite Structures*, **120**, pp. 300-314 (2015).

(Manuscript received October 3, 2017,
accepted for publication January 26, 2018.)

https://doi.org/10.1017/jmech.2018.8 Published online by Cambridge University Press